Coastal Research Library 36

Laith A. Jawad *Editor*

Southern Iraq's Marshes

Their Environment and Conservation

Springer

Coastal Research Library

Volume 36

Series Editor
Charles W. Finkl
Department of Geosciences
Florida Atlantic University
Boca Raton, FL, USA

The aim of this book series is to disseminate information to the coastal research community. The Series covers all aspects of coastal research including but not limited to relevant aspects of geological sciences, biology (incl. ecology and coastal marine ecosystems), geomorphology (physical geography), climate, littoral oceanography, coastal hydraulics, environmental (resource) management, engineering, and remote sensing. Policy, coastal law, and relevant issues such as conflict resolution and risk management would also be covered by the Series. The scope of the Series is broad and with a unique cross-disciplinary nature. The Series would tend to focus on topics that are of current interest and which carry some import as opposed to traditional titles that are esoteric and non-controversial.

Monographs as well as contributed volumes are welcomed.

More information about this series at http://www.springer.com/series/8795

Laith A. Jawad
Editor

Southern Iraq's Marshes

Their Environment and Conservation

Springer

Editor
Laith A. Jawad
School of Environmental and Animal Sciences
Unitec Institute of Technology
Mt Albert, Auckland, New Zealand

ISSN 2211-0577 ISSN 2211-0585 (electronic)
Coastal Research Library
ISBN 978-3-030-66237-0 ISBN 978-3-030-66238-7 (eBook)
https://doi.org/10.1007/978-3-030-66238-7

This Springer imprint is published by the registered company Springer Nature Switzerland AG
The registered company address is: Gewerbestrasse 11, 6330 Cham, Switzerland

Chapter 9
Use of Multispectral and Hyperspectral Satellite Imagery for Monitoring Waterbodies and Wetlands

Mahdi Hasanlou and Seyd Teymoor Seydi

Abstract Timely and accurate change detection (CD) of Earth's surface features is important for understanding interactions between human and natural phenomena. Remote sensing (RS) as the most important information resource plays a role key in monitoring and assessment of the environment. One of most applications of hyperspectral imagery is CD. The hyperspectral imagery provides more details from CD compared to multispectral images. Wetlands are one of the most influential ecosystems in the natural environment for which it is very difficult to find an alternative. The monitoring wetland and waterbody areas based on RS imagery need special techniques due to some limitations (existence noise and condition atmospheric, need to high training data and threshold selection, and complexity of water body areas). Based on these problems it is necessary to CD methods to minimize problems so, this research proposed a framework for hyperspectral CD methods on wetland and water body areas. The proposed method is based on incorporating chronochrome, Z-score analysis, Otsu algorithm, SImplex via Split Augmented Lagrangian (SISAL), Harsanyi–Farrand–Chang (HFC), Pearson correlation coefficient (PCC), and support vector machine (SVM) to detect changes using hyperspectral imagery. The proposed method is applied in four main steps: (1) produce a training data for tuning SVM and kernel parameters, (2) predicted change areas based on a chronochrome algorithm and binary change map obtained using SVM classifier, (3) the amplitude of changes is created by Z-Score analysis and binary change mask, and (4) the multiple change map is produced based on the estimation of number and extraction of endmembers and similarity measure. To evaluate the performance of the proposed method, multi-temporal hyperspectral Hyperion images for Shadegan Wetland were used. The results show high accuracy and low false alarms rate of proposed method methods with an overall accuracy of more than 96%, kappa coefficient of more than 0.82. Besides, the proposed method can provide 'multiple changes' as well as the magnitude of the extracted changes.

M. Hasanlou (✉) · S. T. Seydi
School of Surveying and Geospatial Engineering, College of Engineering, University of Tehran, Tehran, Iran
e-mail: hasanlou@ut.ac.ir; seydi.teymoor@ut.ac.ir

L. A. Jawad (ed.), *Southern Iraq's Marshes*, Coastal Research Library 36,
https://doi.org/10.1007/978-3-030-66238-7_9

Keywords Change detection · Hyperspectral · Wetlands · Multiple-change Map · Shadegan · Wetland

9.1 Introduction

Wetlands are one of the most influential ecosystems in the natural environment for which it is very difficult to find an alternative (White et al. 2015). The US Army Corps of Engineers defined wetlands as "Those areas that are inundated or saturated by surface or groundwater at a frequency and duration sufficient to support, and that under normal circumstances do support, a prevalence of vegetation typically adapted for life in saturated soil conditions." Wetlands cover nearby 6–7% of the earth's surface (Keramitsoglou et al. 2015; Mereta et al. 2012). The wetlands and waterbody areas have provided many vital benefits for the environment which are improving the quality of water, controlling the soil erosion, recharging underground water tables, sustaining against flooding, filtering toxic material and sediments, providing a defense mechanism against sandstorms, and providing food and habitat for wildlife (Romshoo and Rashid 2014; Jiang et al. 2014; Whiteside and Bartolo 2015).

The earth's ecosystems are continuously changing due to natural phenomena (flood, drought) and human activities (urban developing) (Gibbes et al. 2009). The wetland changes originated from some events that included dry seasons, alterations in groundwater, and habitat heterogeneity (Taminskasa et al. 2013; Romshoo and Rashid 2014; Rapinel et al. 2015). Fig. 9.1 presented the change of the Shadegan wetland during 1991 through 2015.

Remote sensing (RS) plays a role key in the monitoring of the changes in the environment, especially in wetlands, on different scales (Mabwoga and Thukral 2014; McCarthy et al. 2015). In fact, RS can provide data from the environment on a large scale and real time with minimum cost and time consumption (Bovolo and Bruzzone 2015; Gómez et al. 2016). These properties have made RS a very effective approach in the fields of earth and environment sciences, especially in change detection applications (Liu 2015; Huang et al. 2017; Storey et al. 2017).

Change detection (CD) is a process that aims to measure the difference between two objects at different times (Lu et al. 2011; Singh 1989). One benefit of the CD is to help manage a system more efficiently by using a multi-temporal dataset (Thonfeld et al. 2016). Also, detection of changes can help us create accurate change models based on past information to avoid disastrous events (Hegazy and Kaloop 2015; Thonfeld et al. 2016). With the development of RS systems, it is possible to obtain data from objects in the high spectral resolution which is known as hyperspectral imagery (George et al. 2014). The high spectral resolution of the data helps with distinguishing objects that seem very similar (Seydi and Hasanlou 2018; Barrett 2013; Smith 2012; Yuen and Richardson 2010).

During recent years, the most relevant studies on CD in wetlands have been using remote sensing data. Sica et al. (2016) study on the Paraná River Delta located in Argentina, where change analysis was performed based on post-classification via the

Fig. 9.1 The change of the Shadegan wetland. (**a**) Landsat image in December, 2015, (**b**) Landsat image in December, 2012, (**c**) Landsat image in December, 1995 and (**d**) Landsat image in December, 1991

supervised method and support vector machine (SVM) classifier. Also, Seydi and Hasanlou (2016) studied the Shadegan wetlands located in Iran. This research proposed a new hybrid method for detecting changes that used a semi-supervised method based on iteratively reweighted multivariate alteration detection (IR-MAD) algorithms, Z-score analysis, and Otsu algorithm. They also used hyperspectral image datasets. In an older study, Ghobadi et al. (2015) studied the Al-Hawizeh wetlands located in the southwest region of the Iran-Iraq border. For change analysis, they used maximum likelihood as the post-classification method and classifier on the Landsat datasets (OLI,[1] MSS,[2] and ETM[3]).

Mousazadeh et al. (2015) studied Anzali wetlands in Iran, where their approach integrated supervised classification using maximum likelihood classifier and zonal and object-oriented image analyses. Also, in their study, Landsat 8 and digital topographic maps datasets were used. In another work, Yang and Yan (2016) conducted a change analysis study on Poyang Lake wetland in China where they used supervised classification procedures using error-correcting output code (ECOC) and SVM algorithm. Also in their study, the hydrological data and remotely sensed data contained TM,[4] ETM, OLI, and TIRS.[5] Gunawardena et al. (2014) monitored the eastern river basin region in Sri Lanka using supervised classification methods and Landsat datasets including ETM+,[6] ALOS[7]-AVNIR-2,[8] and ALOS-PALSAR[9] images. Capella Zanotta et al. (2013) studied the central portion of South American areas, specifically the Brazilian Pantanal. They have investigated automatic hybrid methods based on expectation-maximization (EM) and image difference detection. Also, their method showed improvements in CD efficiency by incorporating morphology operators using Landsat dataset for change analysis. Kayastha et al. (2012) analyzed an area in northern Virginia for CD using Z-score and the tasseled cap algorithm. In their paper, threshold selection was performed based on time series analysis of Landsat ETM datasets.

By considering both the CD methods and the employed datasets in related literature, it can be observed that there are several challenges in CD on wetland regions. Firstly, we can see that the most frequently used procedure for CD is the post-classification method. Secondly, the most widely used image datasets for the application of CD in wetland areas are different types of Landsat imagery. Therefore, there is a lack of research based on hyperspectral images for CD applications. On the other hand, hyperspectral imagery has displayed high potential for many

[1]Operational Land Imager.

[2]Multispectral Scanner System.

[3]Enhanced Thematic Mapper.

[4]Thematic Mapper.

[5]Thermal Infrared Sensor.

[6]Enhanced Thematic Mapper Plus.

[7]Advanced Land Observation Satellite.

[8]Advanced Visible and Near Infrared Radiometer type 2.

[9]Phased Array type L-band Synthetic Aperture Radar.

applications such as classification and CD. Also, several studies have been conducted about this type of imagery (Hasanlou et al. 2015; Kumar and Sinha 2014) which can be considered to be applied in monitoring changes in the wetlands and waterbody areas.

The CD methods using RS imagery can be divided into five groups. The first group includes post-classification comparison-based procedures (Castellana et al. 2007).

The first group of methods includes similarity-based methods where the spectral signature of objects is measured (Adar et al. 2012). The advantages of these methods include the simplicity of implementing them and their low computational cost. Nevertheless, they can be affected by noise and atmospheric conditions, need to threshold selection (Liu 2015; Shah-Hosseini et al. 2015).

The second group is the transformation-based methods where the dataset is transformed from image space to another space (Pieper et al. 2015; Shah-Hosseini et al. 2015; Vongsy 2007). These methods have high potential in processing data with high dimensionality and, thus, high capability in CD. The common transformation-based methods include principal component analysis (PCA) (Vongsy et al. 2009), multivariate alteration detection (MAD) (Nielsena and Müllerb 2003), chronochrome (CC) (Eismann et al. 2008), and cross equalization (CE) (Eismann et al. 2008). The main disadvantage of this method, need to threshold selection and finding informative principles for the extraction of changes.

The third group is the post-classification comparisons which are widely used for detecting changes based on comparing classified images in a pixel by pixel class label manner (Dronova et al. 2011; Lee 2011; Zhao et al. 2010). This group provides "multiple-change" or "from-to" information and is not affected by the atmospheric conditions and sensor differences in the acquisition data. However, prior knowledge for the training set is necessary for this group, which is a big challenge for supervised methods due to the fact that acquiring training sets in multi-temporal datasets can be very difficult (Liu 2015; Shah-Hosseini, Homayouni, and Safari 2015). When using hyperspectral imagery, it is inevitable to use dimension reduction procedures due to the Hughes phenomenon (Samadzadegan et al. 2012). Also, for unsupervised methods, it is necessary to label the classes to be able to analyze the change map (Shah-Hosseini et al. 2015). The accuracies of both supervised and unsupervised CD methods depend on the performance of the utilized classifier algorithm (Liu 2015; Pacifici 2007; Shah-Hosseini et al. 2015). The common supervised post-classification comparison-based methods are maximum likelihood (ML) (Lee 2011; Mousazadeh et al. 2015; Yang and Yan 2016), SVM (Sica et al. 2016; Yang and Yan 2016), and random forest (RF) classifiers (Franklin et al. 2015). Also, the common unsupervised methods are ISODATA[10] classifier (Omo-Irabor 2016), fuzzy C-means (FCM) (Ghosh et al. 2011), and K-means (KM) (Fröjse 2011).

[10]Iterative Self-Organizing Data Analysis Techniques.

The fourth group of CD methods that use hyperspectral imagery uses direct multi-date classification (DMC) based on using one classifier algorithm on stacks of multi-date datasets (Ahlqvist 2008). In this group, due to the utilization of one classifier, the computational cost of classification is low. However, this group of method suffers from drawbacks such as providing little knowledge about the "from-to" information and the fact that for supervised methods, it is necessary to have training sets, and also, they need high computational space for process (Shah-Hosseini et al. 2015; Yuan et al. 2005).

The fifth group is hybrid-based procedures that combine the previous methods in order to achieve new automatic or unsupervised methods (Shah-Hosseini et al. 2015; Bovolo et al. 2012).

We described five CD groups and briefly investigated their pros and cons. Generally, there are many challenges in hyperspectral change detection including (1) the outputs of many segment-based threshold selection procedures are not perfect; therefore, these methods require clear histograms of *change* and *no-change* areas. Also, some CD methods require hyper-parameter tuning, which is necessary to be performed based on experimental knowledge (Shah-Hosseini et al. 2015). (2) Many of the automatic methods do not provide information about the nature of changes but only provide the binary change maps, while multiple-change information is important for decision-making. Moreover, these methods do not provide the amplitude of changes (Hussain et al. 2013; Shah-Hosseini et al. 2015). Also, some CD methods need to have knowledge-based threshold that it is hard to set. (3) However, the post-classification and direct classification methods could provide a multiple-change map or "from-to" information, but these methods are supervised; therefore providing training data is inevitable. However, collection of this training data can be very difficult, and (4) as described in the literature review in the previous section, many of the studies used multispectral dataset to monitor the wetland regions; therefore, there is a lack of research that investigates the capabilities of hyperspectral imagery in CD in wetlands and waterbody areas. Nevertheless, a series of spaceborne sensors (e.g., EnMAP,[11] PRISMA,[12] and HyspIRI[13]) will be launched on a schedule that will increase the availability of hyperspectral imagery with improvement in data quality. With this regard, it is necessary to utilize datasets that provide more detail about changes.

Wetlands are very sensitive ecosystems, which implies that monitoring of their changes is necessary for protecting them. In order to provide a monitoring framework to address this issue, we need to focus on informative image datasets and accurate methods. The CD problem could be solved in a simple framework. There are many novel algorithms proposed by researchers for the detection of changes using hyperspectral imagery that solved CD in a complex framework. Therefore, these novel methods improve the performance of CD, but the CD problems become

[11]Environmental Mapping and Analysis Program.

[12]PRecursore IperSpettrale della Missione Applicativa.

[13]Hyperspectral Infrared Imager.

more complex and hard. So, this research proposed a CD method for hyperspectral imagery on wetland and waterbody areas using conventional algorithms. The main novelty proposed method is a simple theme nonetheless preserved accuracy. In addition, the proposed method could be applied in an automatic framework and provides more details of the nature of changes. The main purpose of this chapter is to propose a CD hybrid method that addresses the previously mentioned CD issues. In addition, this study has a number of minor objectives including (1) sensitivity assessment of different kernel functions on hybrid change detection (HCD) and (2) evaluating the effects of normalization steps on input data on the performance of the SVM classifier. In fact, the proposed method is a new HCD method based on the Otsu algorithm, CC, Z-score, PCC,[14] and SVM and has three phases including (1) global predictor phase, (2) analysis phase, and (3) decision phase. More specifically, the global predictor phase uses CC algorithm for highlighting *change* and *no-change* area; the analysis phase uses the SISAL,[15] HFC,[16] and Z-score analysis for data analysis, and the decision phase uses the SVM classifier, Otsu algorithm, and PCC to obtain the binary change map, the amplitude of change map, and the "multiple-change" information map. The criteria selection mentioned methods in the proposed framework are simple for implementation and robust for the analysis of high-dimensional data. In addition, the source codes of these methods are available and can be found online at http://rslab.ut.ac.ir. This hybrid method benefits from several advantages that distinguish it from other HCD methods including (1) sensitivity to subtle changes with high accuracy and low false alarm rates, (2) providing the "multiple-change" information and amplitudes of changes in addition to binary change map, (3) simple implementation compared to common HCD methods, (4) low computational cost and the ability to process high-dimensional data, (5) no need for training set or its unsupervised framework, and (6) incorporating hyperspectral datasets which have high potentials in most applications especially for CD analysis. The rest of this chapter is organized as follows: Section 9.2 describes the general proposed methodology. The details of the proposed method are presented in Sects. 9.3 and 9.4 presents the experimental results of this method.

9.2 Proposed Hybrid Method

This section investigated the detail of the proposed method. The flowchart of the proposed method is illustrated in Fig. 9.2. The proposed method provides three different change maps that are the binary change map, the magnitude of changes, and the multiple-change map.

[14]Pearson correlation coefficient.

[15]Simplex identification via split augmented Lagrangian.

[16]Harsanyi–Farrand–Chang.

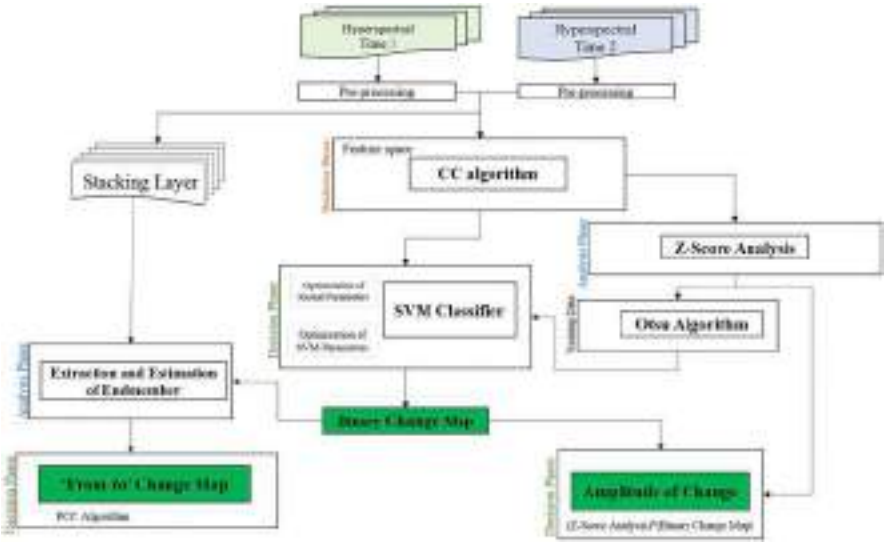

Fig. 9.2 An overview of the proposed method and three blue output boxes

9.2.1 Global Predictor Phase

The main purpose of the predictor phase is to distinguish the *change* pixels from the *no-change* pixels. For this purpose, the CC algorithm was used to highlight the *changing* area from the *no-change* area based on second-order statistics. The result of this phase is a cube data that change areas that differ from *no-change* areas by intensity.

9.2.2 Analysis Phase

The main purpose of this part includes (1) extraction and estimation of endmembers on masked stack data which is performed using HFC and SISAL algorithms, and (2) the output of the CC method is a cubic data; therefore, to aggregate and standardize the output of CC method, the Z-score analysis was applied, and then the single-band data was generated. After extracting and estimating the endmembers, the PCC method is applied to generate the "multiple-change" map. The output of Z-score analysis is used for two purposes: (1) the Z-score analysis is used in combination with the Otsu algorithm in order to generate unsupervised training data, and (2) this method combines binary change maps for extracting the amplitude of change map as a single output.

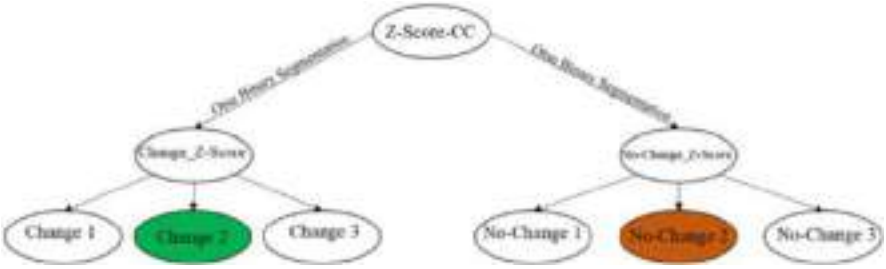

Fig. 9.3 Extraction of training data using iterative Otsu algorithm

9.2.3 Decision Phase

The decision phase is used for (1) locating the *change* and *no-change* pixels (i.e., binary change map), (2) extracting "multiple-change" information, (3) calculating the amplitude of the change map, and (4) automatically generating training data. This phase uses three algorithms: the SVM classifier, the Otsu algorithm, and the PCC algorithm.

9.2.3.1 Training Data Generation

This part explains the automatic production of training data for the SVM classifier by incorporating the Otsu algorithm over the output of CC and the Z-score analysis. After pre-processing of input bitemporal hyperspectral datasets, the first step in the flowchart of the proposed method begins with applying CC transformation and highlighting *change* pixels from *no-change* pixels. The second step of the proposed method is to implement the Otsu algorithm for producing the initial change map. This initial change map contains several *change* pixels mixed with *no-changed* pixel (i.e., unfavorable change pixels) (Fig. 9.3). Therefore, for the initial change map that contains two classes, *change* and *no-change*, the Otsu algorithm is applied once again for each of the previous output classes on the Z-score pixels, and the three classes are divided according to Fig. 9.2.

This process causes more isolation and increases the reliability of *change* and *no-change* pixels. The main reason for dividing the three classes is that the first class for *no-change* class and the third class for change contain many noise pixels because the noise has the minimum value and the maximum value. Therefore, the first class for *no-change* and the third class for *change* are eliminated. The third class for *no-change* and the first class for *change* contain mixed pixels of *change* with *no-change*; therefore, these classes are also removed. In the next step, the pixels whose locations are found via the output of the CC algorithm are selected as the training set for the SVM classifier.

9.2.3.2 Tuning SVM's Kernel Parameters

After producing training data, the parameters of the SVM classifier, including the optimal kernel parameters, are tuned. In this regard, the prepared input datasets are divided into two groups: (1) training data (30% of pixels) and (2) testing data (70% of pixels). The tuning parameters are based on grid search (GS), and the evaluation type is cross-validation that a range is defined for the parameters of kernel and SVM. The SVM classifier is trained using training data based on the defined value of in GS then model made evaluated on training data used criteria such as overall accuracy. The process is repeated until all of the ranges are covered. Finally, the best value of accuracy is equal to tune parameters.

9.2.3.3 Binary Change Map

In the next step, the SVM classifier (based on obtained tune parameters in the previous section) is applied to the output of the CC algorithm. The output of this classifier is a binary change map (i.e., a map with two classes: *change* and *no-change* pixels). The binary change map is determined by assigning each pixel in the image space *change* or *no-change* values. The values of *change* pixels are set to one, and the *no-change* pixels are set to zero.

9.2.3.4 Amplitude of Change

The amplitude of the change map shows the intensity of change. Thus, a high-intensity value represents higher change. The amplitude of the change map is extracted by multiplying the final binary change map by Z-score values, as shown in Fig. 9.4.

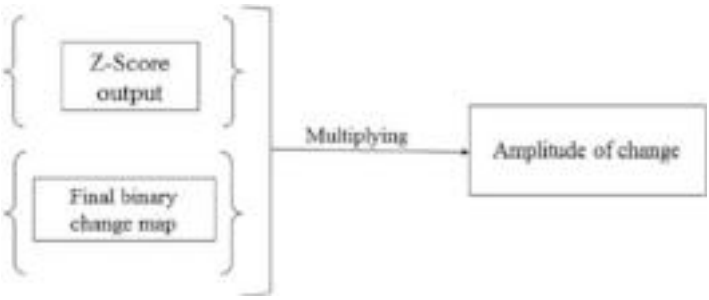

Fig. 9.4 The flowchart of computing amplitude of change

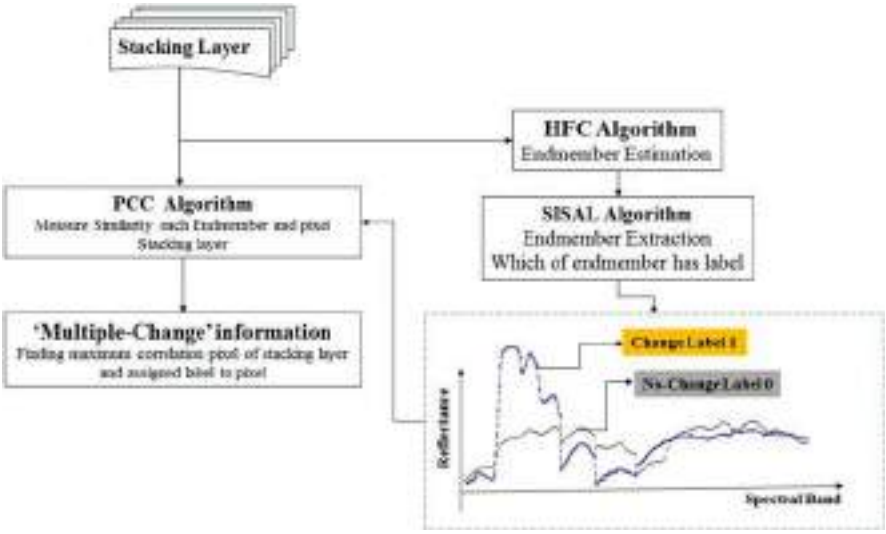

Fig. 9.5 The flowchart retrieving "multiple-change" information

9.2.3.5 Extracting "Multiple-Change" Information

Retrieving accurate "multiple-change" change information is required in many CD analyses (Hussain et al. 2013). In this study, "multiple-change" information is created based on the estimation and extraction of endmembers in the multi-temporal hyperspectral dataset. For this purpose, these four steps are required: (1) masking the *change* area on stack hyperspectral dataset using final binary change map, (2) estimating endmembers by using HFC methods, (3) extracting endmember using SISAL algorithm, and (4) assigning a label for each pixel by finding maximum similarity between pixels of stacking layers and the extracted endmembers by incorporating PCC algorithm. To produce the "multiple-change" map, it is necessary to assign a label to each endmember. Therefore, the PCC algorithm measures the similarity between each endmember and each pixel in stacked hyperspectral data. Usually, assigned labels correspond to endmembers with the highest similarity value. In the next step, pixels with high similarity values related to one of the endmembers are assigned their corresponding labels (Fig. 9.5).

9.3 Methodology

As discussed in the previous section, the proposed hybrid method consists of six main algorithms (Fig. 9.2): (1) chronochrome (CC), (2) Z-score analysis, (3) Otsu algorithm, (4) the SVM classifier, (5) endmember extraction and estimation algorithm, and (6) Pearson correlation coefficient (PCC). Also, the proposed method

consists of three main phases including (a) predictor phase, (b) analysis phase, and (c) decision phase. These algorithms and phases are described in more detail in this section.

9.3.1 Chronochrome

The chronochrome approach, proposed by Stocker and Schaum, provides a prediction based on the joint second-order statistics between the reference and test images (Eismann et al. 2008; Schaum and Stocker 1998). The main purpose of this method is to estimate the background in the test image as a linear function of the reference image and detect the changes in the resulting difference image (Schaum and Stocker 1998; Vongsy 2007). For this purpose, given x, a linear predictor is fitted for y. The centered covariance and cross-covariance are computed before fitting a linear estimation to y-data as a function of the x-data (Eq. 9.1):

$$\mathrm{X} = \langle \mathrm{x}|\mathrm{x}^{\mathrm{t}}\rangle, \mathrm{Y} = \langle \mathrm{y}|\mathrm{y}^{\mathrm{t}}\rangle, \mathrm{C} = \langle \mathrm{y}|\mathrm{x}^{\mathrm{t}}\rangle \tag{9.1}$$

A linear estimate of the y-data from the x-data is (Eq. 9.2):

$$\mathrm{y} = \mathrm{Lx} \tag{9.2}$$

where L is the optimal vector wiener filter solution that it is given by (Eq. 9.3):

$$\mathrm{E} = \left\langle (\mathrm{y} - \mathrm{Lx})(\mathrm{y} - \mathrm{Lx})^{\mathrm{t}} \right\rangle \tag{9.3}$$

Also, E is minimized when $L = CX^{-1}$. Therefore, we have:

$$\mathrm{y} = \mathrm{Lx} = \left(\mathrm{CX}^{-1}\right)\mathrm{x} \tag{9.4}$$

And according to Eqs. 9.3 and 9.4:

$$\varepsilon_{\mathrm{cc}} = (\mathrm{y}) - \left(\left(\mathrm{CX}^{-1}\right)\mathrm{x}\right) \tag{9.5}$$

where ε_{cc} is a change residual image. As depicted in the flowchart of the proposed method in Fig. 9.2, chronochrome is incorporated in the predictor phase on the hyperspectral data.

9.3.2 Z-Score Analysis

The Z-score provides the magnitude and directions of deviation from the mean of the distribution which is introduced in the distribution unit of standard deviation. The Z-score is defined in Eq. 9.6 as follows (Cheadle et al. 2003):

$$\text{modified} - \text{Z\_Score} = \sum_{i=1}^{N} \left((x_i - \text{mean}_i)/\text{std}_i \right) \tag{9.6}$$

In this study, a version of Z-score value is adopted which is, in fact, a normalization that allows us to have the amplitude of change as the output of our proposed method. As stated in Eq . 9.6, the output of this procedure is a single band (Fig. 9.5). The Z-score analysis is then applied to the output of the CC method in the analysis phase as depicted in the flowchart of the proposed method (Figs. 9.2 and 9.6).

9.3.3 Otsu Algorithm

The Otsu algorithm is a group thresholding algorithm that performs image clustering automatically. The idea behind this approach is that the threshold value determines the weight of the variance within the minimum class value. The variance within the class is the variance of the total weight of each defined cluster (Ng 2006; Otsu 1979). In this study, the Otsu algorithm was applied for unsupervised preparation of training data for the SVM classifier according to as shown in the flowchart of the proposed method (Fig. 9.2).

9.3.4 Endmember Extraction

The common method for producing "multiple-change" information is classification, which was discussed in the introduction section. However, this chapter proposes a new procedure for retrieving "from-to" information without applying classification. In this regard, the proposed procedure uses estimation/extraction endmembers as well as the PCC algorithms. On the other hand, many methods are developed for estimating the number of endmembers. We apply the popular HFC method which is based on the distribution of the differences of the eigenvalues of the correlation and the covariance matrices, respectively (Chang and Du 2004). After estimating the

Fig. 9.6 The output of the Z-score analysis has a single band

number of endmembers, endmember extraction begins. Various endmember extraction methods exist in the literature including SISAL (Bioucas-Dias 2009; Keshava 2003; Parente and Plaza 2010). The SISAL algorithm is an unsupervised method for endmember extraction based on fitting a minimum volume simplex to the data subject to a series of constraints. However, it is inevitable to estimate the number of endmembers before using the SISAL algorithm (Bioucas-Dias 2009). In this study, we apply the endmember extraction on the output of the CC algorithm as it can be observed in the flowchart of the proposed method (Fig. 9.2).

9.3.5 Pearson Correlation Coefficient

The PCC is one of the most popular measures for calculating the dependency between two spectral vectors. This measure is widely used in remote sensing applications (Wang 2013). The PCC between spectral random vectors is defined as:

$$\mathrm{PCC} = \frac{\mathrm{cov}(\mathrm{x}, \mathrm{y})}{\sigma_{\mathrm{x}}\sigma_{\mathrm{y}}} \tag{9.7}$$

where x and y represent the target and reference spectra and σ_x and σ_y are the standard deviations of x and y spectral vectors, respectively. This study utilizes PCC in the decision phase for stacking layer data to retrieve the "from-to" information, as depicted in the flowchart of the proposed method (Fig. 9.2).

9.3.6 Support Vector Machine

The SVM is a supervised machine learning algorithm that is commonly used for classification purposes and is based on the statistical learning theory (Vapnik 2013). SVM has recently been applied in the classification of multispectral and hyperspectral remote sensing datasets successfully (George et al. 2014; Melgani and Bruzzone 2004). The main idea behind SVM is to find a hyperplane that maximizes the margin between the two classes (Vapnik 2013). This algorithm has several critical parameters including kernel parameters and the penalty coefficient (C). The popular kernels incorporated in SVM include polynomial, radial bias function, and linear kernels (Gaspar et al. 2012; Hasanlou et al. 2015). Different types of kernels and parameters for SVM are presented in Table 9.1.

This study incorporates the SVM algorithm, in the decision phase, on the output of the CC algorithm to make binary changes as illustrated in the flowchart of the proposed method (Fig. 9.2).

Table 9.1 Different types of kernels and parameters in the SVM classifier

Kernel type	Formula	Estimation parameters	Number parameters
Linear	$k(x, y) = x^T y$	C	1
Polynomial	$k(x, y) = (\gamma x^T y + \beta_0)^d$	d, γ, β_0, C	4
Radial basis function	$k(x, y) = e^{(-\gamma \|x-y\|^2)}$	γ, C	2

9.4 Experiments

In this section, the experimental data and study area are discussed. Also, the results extracted from the proposed method evaluated by qualitative and quantitative criteria are presented. In addition, the change map results of the proposed method are compared with the most common and popular CD algorithms.

9.4.1 Study Area

In this study, three different satellite (i.e., EO-1) hyperspectral image datasets are used for analyzing changes in wetlands and waterbodies as illustrated in Fig. 9.7 and Table 9.2. These datasets have been previously used in many hyperspectral change detection papers (Liu 2015; Seydi and Hasanlou 2016, 2017; Wu et al. 2012), and they can be considered benchmark datasets. The ground truth datasets were developed by the authors through visual analysis and interpretation of the abovementioned researches. Additionally, by using high-resolution image datasets from Google Earth, a detailed visual comparison was carried out. Details and descriptions of each dataset will be presented in the next section. The Hyperion sensor contains 242 spectral bands with wavelengths between 0.4 and 2.5 micrometers and with a spatial resolution of 30 m and a bandwidth of 7.5 km. Hyperion data were obtained at two separate range images using the push broom technology (Jafari and Lewis 2012). One of these spectra was a VNIR range which includes 70 bands between wavelength 356 and 1058 nm and SWIR wavelength consisting of 172 bands between wavelength 852 and 2577 nm ("USGS EO-1" 2017).

9.4.1.1 Poyang Lake (Dataset #1)

The Poyang Lake located in Jiangxi Province is one of largest freshwater resource and biggest floodwater storage wetland areas in China which is located within coordinates 28°24′ to 29°46′N and 115°49′ to 116°46′E (Chan and Xu 2013; Yang and Yan 2016). The extended area of the captured region in the hyperspectral dataset is 232 × 131 pixels. These datasets were acquired from July 16, 2004 and July 27, 2002 (Fig. 9.7a, b).

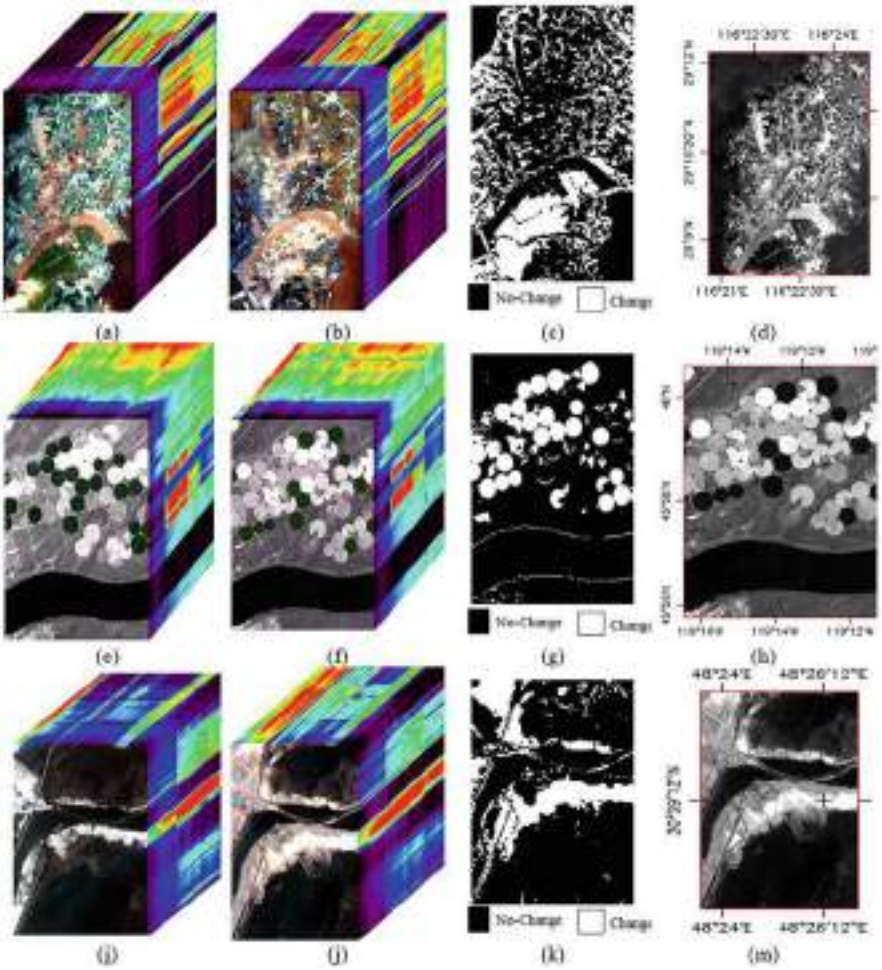

Fig. 9.7 The (**a**) and (**b**) presented false-color composite of the original hyperspectral images acquired in 2002 and 2004 of dataset #1 in China, respectively, (**c**) ground truth, and (**d**) presented geographical location dataset #1. The (**e**) and (**f**) presented false-color composite of the original hyperspectral images acquired in 2004 and 2007 of dataset #2 in the USA, respectively, (**g**) ground truth, and (**h**) presented geographical location dataset #2. The (**i**) and (**j**) present false-color composite of the original hyperspectral images acquired in 2006 and 2006 of dataset #3 in Iran, respectively, (**k**) ground truth, and (**m**) presented geographical location dataset #3

9.4.1.2 Umatilla River (Dataset #2)

The Umatilla River is a gravel-bed river originating in the Blue Mountains of northeastern regions that flows into the Columbia River at Umatilla, OR, USA (Hughes et al. 2006). The extended area of the captured region in the hyperspectral

Table 9.2 The characteristic of datasets in different study areas

Datasets		Acquired date	# of bands	# of pixels	Spatial resolution (m)	Spectral resolution (nm)
Poyang Lake	#1	July 27, 2002	154	232 × 131	30	10
		July 16, 2004				
Umatilla River	#2	May 1, 2004	154	308 × 241	30	10
		May 8, 2007				
Shadegan wetlands	#3	June 6, 2006	154	220 × 123	30	10
		June 29, 2006				

dataset contains 308 × 241 pixels and was acquired on May 1, 2004 and May 8, 2007 (Fig. 9.7c, d).

9.4.1.3 Shadegan Wetlands (Dataset #3)

Shadegan wetland is one of the largest wetlands in Iran. This wetland is created by the downstream part of the river Jarahi and is located at coordinates 30°50′ to 31°00'N and 48°20′ to 49°20′E. The northern section of this wetland includes freshwater, and the salty waterbody is located in the southern part. Also, this wetland is home to different types of plants. The extent of the desired region extracted from EO-1 Hyperion satellite hyperspectral images was 220 × 123 pixels. In this area, we incorporate two multi-temporal datasets acquired on June 29 and June 6, 2006. In Fig. 9.7e, f, a false-color composite of hyperspectral Shadegan wetland images for two different times is illustrated.

9.4.2 Implementation

Data pre-processing plays an important role before the beginning of the main process and can be divided into two categories (Jafari and Lewis 2012): spectral and spatial correction. The pre-processing step starts with spectral correction processing; then spatial correction is applied. The first step of pre-processing consists of omitting no-data bands. In this regard, 44 bands (1–7, 58–76, and 225–242) were removed from our imagery (Jafari and Lewis 2012; Scheffler and Karrasch 2013). Also, of the 198 initial bands, two noisy bands including 77 and 78 as well as a number of other bands were removed (Datt et al. 2003; Khurshid et al. 2006). Therefore, 154 bands were selected in total as the input dataset for the proposed change detection method.

Table 9.3 The results obtained from tuning SVM classifier and kernels parameters in different hyperspectral datasets

Datasets	Normalize	Linear		Polynomial					Radial bias function		
		C	# of SV	C	# of SV	γ	d	β_0	C	# of SV	γ
#1	Yes	2–8	210	2–3	16	2–7	3	1	2–6	17	2–7
	No	23	54	2–7	5	21: 220	3	1	2–3	48	2–7
#2	Yes	2–13	408	2–3	13	2–6	3	1	24	125	2–12
	No	25	206	2–6	6	20: 215	3	1	26	125	2–12
#3	Yes	29	5	2–6	608	2–9	3	1	23	65	2–3
	No	25	15	2–9	4	2–9: 29	3	1	25	61	2–5

In the second step, pixels in sample 129 and all lines are shifted to sample 256 in the shortwave infrared (SWIR) spectral bands (Goodenough et al. 2003; Jafari and Lewis 2012; Li et al. 2008). The third step is de-noising, de-striping, and also removing the zero-line by utilizing means and the global approach (Jafari and Lewis 2012; Scheffler and Karrasch 2013). The fourth pre-processing step is a radiometric correction. To achieve this goal, the digital number (DN) values of pixels are converted to physical radiance. The fifth step of the pre-processing is an atmospheric correction, which we used the FLAASH[17] model. The final step of the pre-processing of the hyperspectral dataset is a spatial correction. The accuracy of the geometric correction (RMSE) was less than 0.4 pixel for all three datasets.

As already discussed, the outputs of the proposed method are (1) binary change map, (2) the amplitude of change map, and (3) the "multiple-change" information map. The structure and details of the proposed method are illustrated in Fig. 9.2. This work considered a type of kernel that is widely utilized in the remote sensing community (Liu and Parhi 2016; Ring and Eskofier 2016; Sakthivel et al. 2016; Shah-Hosseini et al. 2015). To tune and select optimized SVM parameters (i.e., gamma (γ) and penalty coefficient (C)), we performed a CV with GS procedures (Gu et al. 2017; Varma and Simon 2006). Also, to have efficient kernel normalization, training and testing data were applied. In the normalization procedure, the data is mapped to values within the *[0,1]* span. The minimum and maximum values were selected based on the minimum and maximum of training data. Table 9.3 presents the results obtained from tuning parameters for kernel and SVM (i.e., the number of support vectors (# of SV), penalty coefficient (C), and gamma (γ) parameter) for three datasets. In addition, this table presented the optimum values for SVM and kernels in two scenarios: normalize and un-normalize.

[17]Fast Line-of-sight Atmospheric Analysis of Spectral Hypercubes.

Table 9.4 Performance of the SVM classifier using a type of kernels in different hyperspectral datasets

Datasets		#1		#2		#3	
Kernel function	Normalize	Overall accuracy (%)	Kappa	Overall accuracy (%)	Kappa	Overall accuracy (%)	Kappa
Linear	Yes	96.77	0.927	97.16	0.907	92.73	0.756
	No	94.68	0.884	97.05	0.906	92.84	0.760
Polynomial	Yes	90.83	0.806	97.10	0.908	96.17	0.885
	No	88.11	0.705	94.75	0.816	89.57	0.628
Radial bias function	Yes	97.40	0.941	97.16	0.908	96.44	0.892
	No	96.65	0.922	97.16	0.908	96.34	0.890

Table 9.5 The number of endmembers and false alarm probability (Pf) for different datasets

Datasets	# of endmembers	P_f
#1	6	10–3
#2	4	10–3
#3	3	10–5

Table 9.4 presented the performance of the SVM classifier using a type of kernels in different hyperspectral datasets. The results show the RBF kernel has the best performance for three datasets. Also, the normalizing dataset improved the accuracy result of the CD.

As mentioned in the above section, to have "multiple-change" information in this study, we used HFC, SISAL, and PCC algorithms. In the HFC algorithm, false alarm probability (P_f) parameters are assigned. A number of endmembers and false alarm probability are listed in Table 9.5.

As we have already discussed in the previous sections, it is essential to compare and check the performance of the proposed method with common and popular CD methods. In this regard, we incorporated ground truth data for all three datasets to compute the validation criteria. In this paper, both quantitative and qualitative criteria were used for comparing the result. The popularly employed CD methods are principal component analysis (PCA) (Adar et al. 2011; Vongsy et al. 2009; Vongsy 2007), cross equalization (CE) (Adar et al. 2011; Eismann et al. 2008), spectral angle mapper (SAM) (Adar et al. 2011), subspace-based (SSB) (Wu et al. 2013), multivariate alteration detection (MAD) (Nielsena and Müllerb 2003), and iterative reweight-MAD (IR-MAD) (Nielsen 2007; Seydi and Hasanlou 2016). All of these methods require assigning suitable thresholds. In this study, unsupervised segmentation by incorporating the Otsu algorithm was used to set these thresholds.

Therefore, by considering the optimum kernel parameters (Table 9.3) for SVM classification for all datasets (#1, #2, and #3), the proposed method begins. Figure 9.8 shows a visual analysis of the proposed method and other CD methods on multi-temporal hyperspectral datasets #1. As it is clear in Fig. 9.8, the proposed method can detect all changes and provide information about the feature changes including

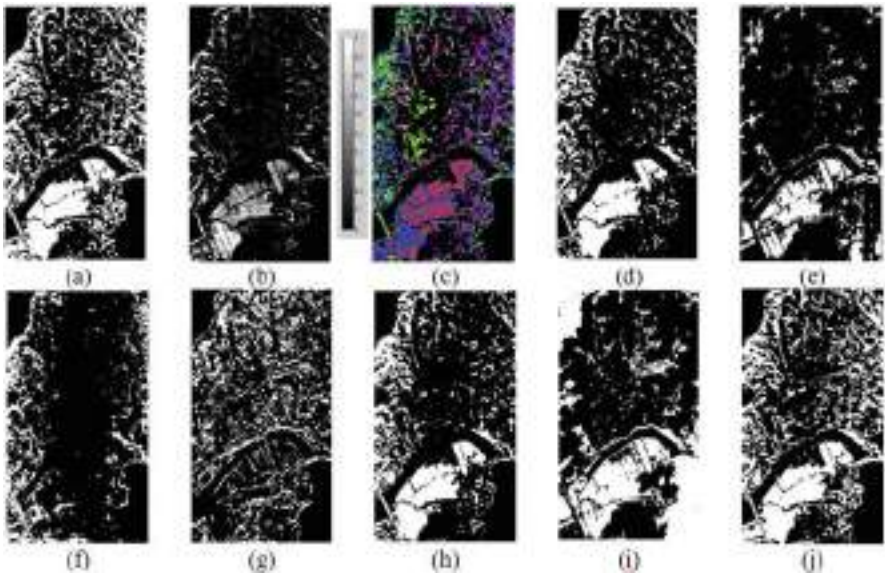

Fig. 9.8 The results of CD methods for dataset #1. (**a**) Proposed method, binary change map; (**b**) proposed method, amplitude of change map; (**c**) proposed method, "from-to" map; (**d**) CE; (**e**) SSB; (**f**) IR-MAD; (**g**) MAD; (**h**) PCA; (**i**) SAM; and (**j**) ground truth

the "multiple-change" change map as well as the amplitude of changes in the map. This observation empirically proves that the proposed method nearly detects all of the changes compared to the other techniques. In the endmember extraction section, we described that the SISAL and HFC methods were used to obtain the "multiple-change" map. Hence, six classes detected and produced the "multiple-change" change map (Fig. 9.8c) for dataset #1. Figure 9.8b shows the amplitude of changes where the changing intensity is clearly highlighted.

The same computational approach is applied to dataset #2. Figure 9.9 shows changes of Umatilla River where there are many land cover change types in areas that contain different agricultural fields. Also, in this figure, there are low changes in the edges of the river. In this dataset (#2), the "multiple-change" change map has four classes that are detected by the proposed method (Fig. 9.9c). In Fig. 9.9, some algorithms show a certain level of sensitivity to the waterbody area such as the results presented in Fig. 9.9e, f, g**.** On the other hand, one can clearly observe from the results (Fig. 9.9a–c) that the proposed method has excellent performance compared to other approaches in this area.

Similarly, Fig. 9.10 presents the results of the CD methods on Shadegan wetland (dataset #3). In this region, the main changes are originated from seasonal changes in the water level. The proposed method can find three different classes for the changing area (Fig. 9.10c). As it is clear from the figure, the similarity-based methods such as SAM technique are not suitable for monitoring the changes due to the extraction of false alarm pixels.

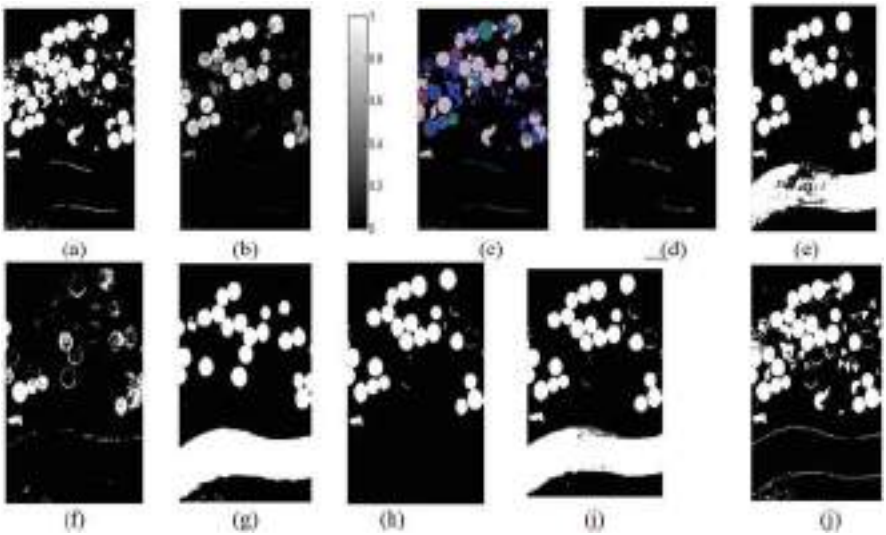

Fig. 9.9 The results of CD methods for dataset #2. (**a**) Proposed method, binary change map; (**b**) proposed method, amplitude of change map; (**c**) proposed method, "from-to" map; (**d**) CE; (**e**) SSB; (**f**) IR-MAD; (**g**) MAD; (**h**) PCA; (**i**) SAM; and (**j**) ground truth

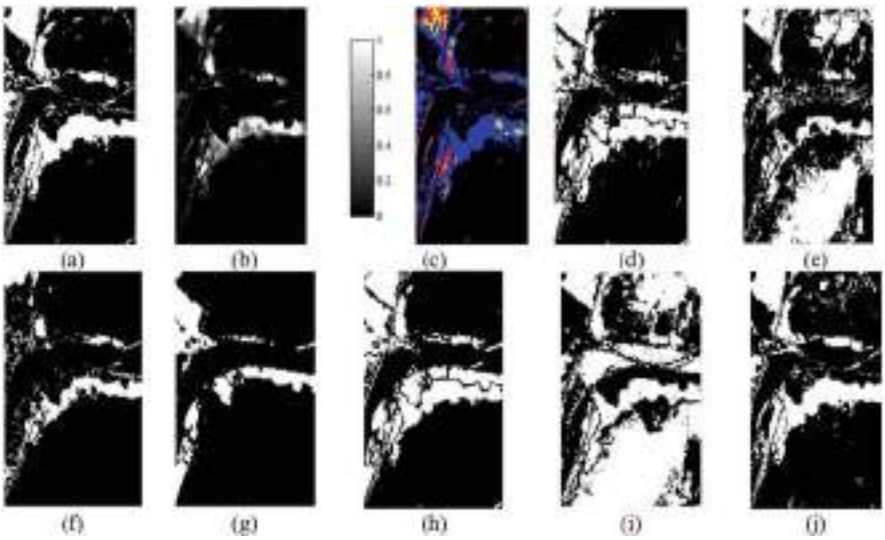

Fig. 9.10 The results of CD methods for dataset #3. (**a**) Proposed method, binary change map; (**b**) proposed method, amplitude of change map; (**c**) proposed method, "from-to" map; (**d**) CE; (**e**) SSB; (**f**) IR-MAD; (**g**) MAD; (**h**) PCA; (**i**) SAM; and (**j**) ground truth

Table 9.6 Performance of the proposed method and other common CD methods for all hyperspectral datasets

Datasets	Indices	SAM	IR-MAD	MAD	CE	SBB	PCA	Proposed method
#1	Overall	66.01	67.07	65.76	88.89	73.11	89.58	97.40
	Kappa	0.223	0.038	0.143	0.727	0.299	0.747	0.941
#2	Overall	75.53	83.85	67.51	93.70	77.855	93.24	97.16
	Kappa	0.371	0.304	0.159	0.778	0.400	0.756	0.907
#3	Overall	52.42	86.06	69.53	83.44	63.86	81.81	96.42
	Kappa	0.111	0.498	0.092	0.527	0.144	0.485	0.890

After the primary observational analysis, we perform a numerical evaluation. In this regard, two common measures are used for evaluating the performance and accuracy of CD methods which include overall accuracy and kappa coefficient. All implemented CD methods are supervised, and their related accuracy is usually computed by examining the best threshold value selection. That means each threshold has a correlation with the accuracy, and maximum accuracy is considered as the final accuracy. Table 9.6 presents the accuracy of the proposed method for the RBF kernel and other CD techniques.

We can clearly observe the superiority of the proposed method compared to other methods in all three different hyperspectral datasets in Table 9.5. Also, as presented in Table 9.5, the PCA and CE methods have efficiencies close to the proposed method, especially for hyperspectral dataset #1 and hyperspectral dataset #2. The IR-MAD algorithm has good performance compared to the MAD algorithm. SAM and SSB have low performance due to sensitivity to noise and atmospheric conditions. These methods utilizing continuous spectral signatures nevertheless, this issue caused to don't suitable for wetland and waterbody change detection using hyperspectral imagery.

This investigation proposed a new change detection method on hyperspectral imagery which included observational and numerical analysis and comparison with other common HCD methods. The proposed method provides three different outputs, which provide more detail about the changes, and thus helps in understanding the changes, while the other CD methods do not give three outputs together. The lecture review in the introduction section and the type of change detection method in five main groups are considered. The challenges and advantages are discussed, and the results of CD certified these issues of CD methods. In addition, more details of visual and numerical analysis show that (1) the hyperspectral imagery has a high capability for CD in waterbodies and wetlands; (2) the CE methods provide better results among common HCD methods; (3) some techniques, such as SSB and SAM, are not suitable for waterbody change detection due to their high sensitivity; (4) the proposed method has the highest accuracy for all employed datasets; therefore, it is efficient for waterbody area; and (5) finally, the proposed methods provide more detail of changes that can help improve the decision-making process.

9.5 Conclusion

Wetlands are critical ecosystems where changes occur frequently and widely. Therefore, creating a framework for monitoring the changes in these ecosystems is essential. In this regard, studying methods that are able to perform accurate change detection in these areas is crucial. This investigation presents a new hybrid method for achieving precise and informative change maps using hyperspectral imagery without requiring prior knowledge of the wetlands and waterbody area. We first discussed all the issues related to CDs using hyperspectral imagery. Therefore, a new change detection method was proposed to address these issues. The proposed hybrid method uses four groups of CD methods to enhance the content and quality of final CD results. The experiments were applied to three real hyperspectral datasets on wetland and waterbody areas from different regions and countries. The output results showed the following: (1) the hyperspectral imagery has high potential to monitoring and assessment of wetland and waterbody areas, however, for this purpose, need special techniques; (2) the visual and numerical analysis proved the excellent performance of the proposed method for hyperspectral change detection compared to other methods; (3) superiority of the proposed unsupervised method without requiring prior knowledge of changes, while some CD methods need training data or setting parameters; (4) the fact that this method can provide binary change map as well as the information about change structure ("multiple-change" map) and also the amplitude map; (5) the use of normalize data and RBF kernel improved the accuracy CD, significantly; and (6) the fact that the implementation of the proposed method is simple and has high efficiency in comparison to other famous and commonly used CD methods like PCA, CE, IR-MAD, SSB, and SAM.

References

Adar S, Notesco G, Brook A, Livne I, Rojik P, Kopackova V et al (2011, October) Change detection over Sokolov open-pit mining area, Czech Republic, using multi-temporal HyMAP data (2009–2010). In: Image and signal processing for remote sensing XVII, vol 8180. International Society for Optics and Photonics, p 81800T

Adar S, Shkolnisky Y, Dor EB (2012, July) New approach for spectral change detection assessment using multistrip airborne hyperspectral data. In: Geoscience and remote sensing symposium (IGARSS), 2012 IEEE International. IEEE, pp 4966–4969

Ahlqvist O (2008) Extending post-classification change detection using semantic similarity metrics to overcome class heterogeneity: a study of 1992 and 2001 US National Land Cover Database changes. Remote Sens Environ 112(3):1226–1241

Barrett EC (2013) Introduction to environmental remote sensing. Routledge

Bioucas-Dias JM (2009, August) A variable splitting augmented Lagrangian approach to linear spectral unmixing. In: Hyperspectral image and signal processing: evolution in remote sensing, 2009. WHISPERS'09. First workshop on. IEEE, pp 1–4

Bovolo F, Bruzzone L (2015) The time variable in data fusion: a change detection perspective. IEEE Geosci Remote Sens Mag 3(3):8–26

Bovolo F, Marchesi S, Bruzzone L (2012) A framework for automatic and unsupervised detection of multiple changes in multitemporal images. IEEE Trans Geosci Remote Sens 50(6):2196–2212
Castellana L, D'Addabbo A, Pasquariello G (2007) A composed supervised/unsupervised approach to improve change detection from remote sensing. Pattern Recogn Lett 28(4):405–413
Chan KKY, Xu B (2013) Perspective on remote sensing change detection of Poyang Lake wetland. Ann GIS 19(4):231–243
Chang CI, Du Q (2004) Estimation of number of spectrally distinct signal sources in hyperspectral imagery. IEEE Trans Geosci Remote Sens 42(3):608–619
Cheadle C, Cho-Chung YS, Becker KG, Vawter MP (2003) Application of z-score transformation to Affymetrix data. Appl Bioinforma 2(4):209–217
Datt B, McVicar TR, Van Niel TG, Jupp DL, Pearlman JS (2003) Preprocessing EO-1 Hyperion hyperspectral data to support the application of agricultural indexes. IEEE Trans Geosci Remote Sens 41(6):1246–1259
Dronova I, Gong P, Wang L (2011) Object-based analysis and change detection of major wetland cover types and their classification uncertainty during the low water period at Poyang Lake, China. Remote Sens Environ 115(12):3220–3236
Eismann MT, Meola J, Hardie RC (2008) Hyperspectral change detection in the presence of diurnal and seasonal variations. IEEE Trans Geosci Remote Sens 46(1):237–249
Franklin SE, Ahmed OS, Wulder MA, White JC, Hermosilla T, Coops NC (2015) Large area mapping of annual land cover dynamics using multitemporal change detection and classification of Landsat time series data. Can J Remote Sens 41(4):293–314
Fröjse L (2011) Multitemporal satellite images for urban change detection
Gaspar P, Carbonell J, Oliveira JL (2012) On the parameter optimization of Support Vector Machines for binary classification. J Integr Bioinform 9(3):33–43
George R, Padalia H, Kushwaha SPS (2014) Forest tree species discrimination in western Himalaya using EO-1 Hyperion. Int J Appl Earth Obs Geoinf 28:140–149
Ghobadi Y, Pradhan B, Shafri HZ, bin Ahmad N, Kabiri K (2015) Spatio-temporal remotely sensed data for analysis of the shrinkage and shifting in the Al Hawizeh wetland. Environ Monit Assess 187(1):1–17. https://doi.org/10.1007/s10661-014-4156-0
Ghosh A, Mishra NS, Ghosh S (2011) Fuzzy clustering algorithms for unsupervised change detection in remote sensing images. Information Sciences 181:699–715. https://doi.org/10.1016/j.ins.2010.10.016
Gibbes C, Southworth J, Keys E (2009) Wetland conservation: change and fragmentation in Trinidad's protected areas. Geoforum 40(1):91–104
Gómez C, White JC, Wulder MA (2016) Optical remotely sensed time series data for land cover classification: a review. ISPRS J Photogramm Remote Sens 116:55–72
Goodenough DG, Dyk A, Niemann KO, Pearlman JS, Chen H, Han T et al (2003) Processing Hyperion and ALI for forest classification. IEEE Trans Geosci Remote Sens 41(6):1321–1331. https://doi.org/10.1109/TGRS.2003.813214
Gu B, Sheng VS, Tay KY, Romano W, Li S (2017) Cross Validation Through Two-Dimensional Solution Surface for Cost-Sensitive SVM. IEEE Trans Pattern Anal Mach Intell 39(6):1103–1121
Gunawardena A, Fernando T, Takeuchi W, Wickramasinghe CH, Samarakoon L (2014) Identification, evaluation and change detection of highly sensitive wetlands in South-Eastern Sri Lanka using ALOS (AVNIR2, PALSAR) and Landsat ETM+ data. In: IOP conference series: earth and environmental science, vol 20. IOP Publishing, p 012050
Hasanlou M, Samadzadegan F, Homayouni S (2015) SVM-based hyperspectral image classification using intrinsic dimension. Arab J Geosci 8(1):477–487
Hegazy IR, Kaloop MR (2015) Monitoring urban growth and land use change detection with GIS and remote sensing techniques in Daqahlia governorate Egypt. Int J Sustain Built Environ 4(1):117–124
Huang S, Ramirez C, Kennedy K, Mallory J, Wang J, Chu C (2017) Updating land cover automatically based on change detection using satellite images: case study of national forests in Southern California. GISci Remote Sens:1–20

Hughes ML, McDowell PF, Marcus WA (2006) Accuracy assessment of georectified aerial photographs: implications for measuring lateral channel movement in a GIS. Geomorphology 74(1–4):1–16

Hussain M, Chen D, Cheng A, Wei H, Stanley D (2013) Change detection from remotely sensed images: From pixel-based to object-based approaches. ISPRS J Photogramm Remote Sens 80:91–106

Jafari R, Lewis MM (2012) Arid land characterisation with EO-1 Hyperion hyperspectral data. Int J Appl Earth Obs Geoinf 19:298–307

Jiang F, Qi S, Liao F, Ding M, Wang Y (2014) Vulnerability of Siberian crane habitat to water level in Poyang Lake wetland, China. GISci Remote Sens 51(6):662–676

Kayastha N, Thomas V, Galbraith J, Banskota A (2012) Monitoring wetland change using inter-annual landsat time-series data. Wetlands 32(6):1149–1162

Keramitsoglou I, Stratoulias D, Fitoka E, Kontoes C, Sifakis N (2015) A transferability study of the kernel-based reclassification algorithm for habitat delineation. Int J Appl Earth Obs Geoinf 37:38–47

Keshava N (2003) A survey of spectral unmixing algorithms. Lincoln Lab J 14(1):55–78

Khurshid KS, Staenz K, Sun L, Neville R, White HP, Bannari A, Champagne CM et al (2006) Preprocessing of EO-1 Hyperion data. Can J Remote Sens 32(2):84–97

Kumar L, Sinha P (2014) Mapping salt-marsh land-cover vegetation using high-spatial and hyperspectral satellite data to assist wetland inventory. GISc Remote Sens 51(5):483–497

Lee S (2011) Detecting wetland change through supervised classification of Landsat Satellite Imagery within the Tunkwa Watershed of British Columbia, Canada. Retrieved January 10, 2017, from http://www.diva-portal.org/smash/record.jsf?pid=diva2:681571

Li H, Zhang D, Zhang Y, Xu Y (2008) Research of image preprocessing methods for EO-1 Hyperion hyperspectral data in tidal flat area. Geoinformatics:71471G–71471G

Liu S (2015) Advanced techniques for automatic change detection in multitemporal hyperspectral images. University of Trento. Retrieved January 10, 2017, from http://eprints-phd.biblio.unitn.it/1393/

Liu Y, Parhi KK (2016) Computing RBF kernel for SVM classification using stochastic logic. In: Signal Processing Systems (SiPS), 2016 IEEE International Workshop on. IEEE, pp 327–332

Lu D, Moran E, Hetrick S, Li G (2011) Land-use and land-cover change detection. In: Advances in environmental remote sensing sensors, algorithms, and applications. CRC Press Taylor & Francis Group, New York, pp 273–290

Mabwoga SO, Thukral AK (2014) Characterization of change in the Harike wetland, a Ramsar site in India, using landsat satellite data. Springerplus 3(1):576

McCarthy MJ, Merton EJ, Muller-Karger FE (2015) Improved coastal wetland mapping using very-high 2-meter spatial resolution imagery. Int J Appl Earth Obs Geoinf 40:11–18

Melgani F, Bruzzone L (2004) Classification of hyperspectral remote sensing images with support vector machines. IEEE Trans Geosci Remote Sens 42(8):1778–1790

Mereta ST, Boets P, Bayih AA, Malu A, Ephrem Z, Sisay A, Endale H et al (2012) Analysis of environmental factors determining the abundance and diversity of macroinvertebrate taxa in natural wetlands of Southwest Ethiopia. Eco Inform 7(1):52–61

Mousazadeh R, Ghaffarzadeh H, Nouri J, Gharagozlou A, Farahpour M (2015) Land use change detection and impact assessment in Anzali international coastal wetland using multi-temporal satellite images. Environ Monit Assess 187(12):1–11

Ng H-F (2006) Automatic thresholding for defect detection. Pattern Recogn Lett 27(14):1644–1649

Nielsen AA (2007) The regularized iteratively reweighted MAD method for change detection in multi-and hyperspectral data. IEEE Trans Image Process 16(2):463–478

Nielsena AA, Müllerb A (2003) Change detection by the MAD method in hyperspectral image data. Retrieved May 9, 2017, from http://citeseerx.ist.psu.edu/viewdoc/summary?doi=10.1.1.608.8367

Omo-Irabor OO (2016) A comparative study of image classification algorithms for landscape assessment of the Niger Delta Region. J Geogr Inf Syst 8(02):163

Otsu N (1979) A threshold selection method from gray-level histograms. IEEE Trans Syst Man Cybern 9(1):62–66

Pacifici F (2007) Change detection algorithms: State of the art. URL: http://www.disp.uniroma2.it/earth_observation/pdf/CD-Algorithms.pdf. Accessed 4 Nov 2011

Parente M, Plaza A (2010) Survey of geometric and statistical unmixing algorithms for hyperspectral images. In: Hyperspectral image and signal processing: evolution in remote sensing (WHISPERS), 2010 2nd workshop on. IEEE, pp 1–4

Pieper M, Manolakis D, Cooley T, Brueggeman M, Weisner A, Jacobson J (2015) New insights and practical considerations in hyperspectral change detection. In: 2015 IEEE International Geoscience and Remote Sensing Symposium (IGARSS). IEEE, pp 4161–4164

Rapinel S, Hubert-Moy L, Clément B (2015) Combined use of LiDAR data and multispectral earth observation imagery for wetland habitat mapping. Int J Appl Earth Obs Geoinf 37:56–64

Ring M, Eskofier BM (2016) An approximation of the Gaussian RBF kernel for efficient classification with SVMs. Pattern Recogn Lett 84:107–113

Romshoo SA, Rashid I (2014) Assessing the impacts of changing land cover and climate on Hokersar wetland in Indian Himalayas. Arab J Geosci 7(1):143–160

Sakthivel NR, Saravanamurugan S, Nair BB, Elangovan M, Sugumaran V (2016) Effect of kernel function in support vector machine for the fault diagnosis of pump. J Eng Sci Technol 11(6):826–838

Samadzadegan F, Hasani H, Schenk T (2012) Simultaneous feature selection and SVM parameter determination in classification of hyperspectral imagery using ant colony optimization. Can J Remote Sens 38(2):139–156

Schaum A, Stocker A (1998) Long-interval chronochrome target detection. In: Proc. 1997 International symposium on spectral sensing research, pp 1760–1770

Scheffler D, Karrasch P (2013) Preprocessing of hyperspectral images: a comparative study of destriping algorithms for EO1-hyperion. In: Image and signal processing for remote sensing XIX, vol 8892. International Society for Optics and Photonics, p 88920H

Seydi ST, Hasanlou M (2016) Novel wetland and water body change detection using multitemporal hyperspectral imagery. In: Presented at the International Water Conference 2016 on Water Resources in Arid Areas. Springer, Oman

Seydi ST, Hasanlou M (2017) A new land-cover match-based change detection for hyperspectral imagery. Eur J Remote Sens 50(1):517–533

Seydi ST, Hasanlou M (2018) Sensitivity analysis of pansharpening in hyperspectral change detection. Applied Geomatics:1–11

Shah-Hosseini R, Homayouni S, Safari A (2015) A hybrid kernel-based change detection method for remotely sensed data in a similarity space. Remote Sens 7(10):12829–12858

Sica YV, Quintana RD, Radeloff VC, Gavier-Pizarro GI (2016) Wetland loss due to land use change in the Lower Paraná River Delta, Argentina. Sci Total Environ 568:967–978

Singh A (1989) Review article digital change detection techniques using remotely-sensed data. Int J Remote Sens 10(6):989–1003

Smith R (2012) Introduction to hyperspectral imaging, MicroImages Inc. Mentor, OH. Retrieved from http://www.microimages.com/documentation/Tutorials/hyprspec.pdf

Storey EA, Stow DA, Coulter LL, Chen C (2017) Detecting shadows in multi-temporal aerial imagery to support near-real-time change detection. GISci Remote Sens:1–18

Taminskasa, J., Petro\liusa R, \Limanauskienėa R, Satkūnasb J, Linkevičienėa R (2013) Prediction of change in wetland habitats by groundwater: case study in Northeast Lithuania. Estonian J Earth Sci 62(2):57ø e72

Thonfeld F, Feilhauer H, Braun M, Menz G (2016) Robust Change Vector Analysis (RCVA) for multi-sensor very high resolution optical satellite data. Int J Appl Earth Obs Geoinf 50:131–140

Varma S, Simon R (2006) Bias in error estimation when using cross-validation for model selection. BMC Bioinform 7(1):91

Vapnik V (2013) The nature of statistical learning theory. Springer, Heidelberg

Vongsy KM (2007). Change detection methods for hyperspectral imagery. Wright State University. Retrieved January 10, 2017, from https://etd.ohiolink.edu/!etd.send_file?accession=wright1184010751&disposition=attachment

Vongsy K, Mendenhall MJ, Hanna PM, Kaufman J (2009) Change detection using synthetic hyperspectral imagery. In: Hyperspectral image and signal processing: evolution in remote sensing, 2009. WHISPERS'09. First workshop on. IEEE, pp 1–4. Retrieved May 21, 2017, from http://ieeexplore.ieee.org/abstract/document/5289016/

Wang J (2013) Pearson correlation coefficient. In: Encyclopedia of systems biology. Springer, pp 1671–1671. Retrieved January 28, 2017, from http://link.springer.com/content/pdf/10.1007/978-1-4419-9863-7_372.pdf

White L, Brisco B, Dabboor M, Schmitt A, Pratt A (2015) A collection of SAR methodologies for monitoring wetlands. Remote Sens 7(6):7615–7645

Whiteside TG, Bartolo RE (2015) Use of WorldView-2 time series to establish a wetland monitoring program for potential offsite impacts of mine site rehabilitation. Int J Appl Earth Obs Geoinf 42:24–37

Wu C, Zhang L, Du B (2012) Targeted change detection for stacked multi-temporal hyperspectral image. In: Hyperspectral image and signal processing (WHISPERS), 2012 4th workshop on. IEEE, pp 1–4. Retrieved July 31, 2017, from http://ieeexplore.ieee.org/abstract/document/6874282/

Wu C, Du B, Zhang L (2013) A subspace-based change detection method for hyperspectral images. IEEE J Sel Top Appl Earth Observ Remote Sens 6(2):815–830

Yang Y, Yan Z (2016) Monitoring and Analyzing of Poyang Lake Wetland Land Use Change Based on RS and GIS. In: Geo-informatics in resource management and sustainable ecosystem. Springer, pp 213–221

Yuan F, Sawaya KE, Loeffelholz BC, Bauer ME (2005) Land cover classification and change analysis of the Twin Cities (Minnesota) Metropolitan Area by multitemporal Landsat remote sensing. Remote Sens Environ 98(2):317–328

Yuen PW, Richardson M (2010) An introduction to hyperspectral imaging and its application for security, surveillance and target acquisition. Imaging Sci J 58(5):241–253

Zanotta DC, Zani H, Shimabukuro YE (2013) Automatic detection of burned areas in wetlands by remote sensing multitemporal images. In: Geoscience and Remote Sensing Symposium (IGARSS), 2013 IEEE International. IEEE, pp 1959–1962

Zhao H, Cui B, Zhang H, Fan X, Zhang Z, Lei X (2010) A landscape approach for wetland change detection (1979-2009) in the Pearl River Estuary. Procedia Environ Sci 2:1265–1278